Three-body recombination of cold helium atoms

H. Suno and B. D. Esry
Department of Physics, Cardwell Hall, Kansas State University, Manhattan, Kansas 66506

Chris H. Greene
Department of Physics and JILA, University of Colorado, Boulder, Colorado 80309

James P. Burke, Jr.
National Institute of Standards and Technology, Gaithersburg, Maryland 20899
(Received 30 October 2001; published 8 April 2002)

We have developed a method for calculating the rates for three-body recombination of cold atoms. This method allows us to treat not only zero total angular momentum, $J=0$, states but also $J>0$ states, so that recombinations at nonzero collision energies can be considered. Our method is applied to ground-state helium atoms ^{4}He, using a realistic interaction potential. In addition, we obtain the rates for collision induced dissociation.

DOI: 10.1103/PhysRevA.65.042725 PACS number(s): 34.50.−s, 34.10.+x

I. INTRODUCTION

Three-body recombination, a three-body collision in which two atoms form a bound state and the third one carries away the binding energy, is an important loss mechanism for Bose-Einstein condensates. This process is also important in nuclear physics and in the chemical dynamics of combustion and gas-phase systems. Only recently have nonperturbative, quantum-mechanical investigations been carried out. Previous investigations [1–5] have predicted that the rate for ultracold three-body recombination of identical bosons scales generally like a^4 (where a is the two-body scattering length). All of these calculations, using model interaction potentials, have been carried out in the ultracold (or the zero-temperature) limit, where only the transitions from the lowest three-body continuum channel to the two-body recombination channels with zero total angular momentum, $J=0$, need to be taken into account.

This work extends the previous investigations in Ref. [1]. We will take into account not only $J=0$ states, but also $J>0$ states. Thus, the recombination rates K_3 at nonzero collision energies can be accurately calculated for the first time. We consider the simple case of ground-state helium atoms (for which the dimer has only one bound state) using a realistic interaction potential [6]. This work allows a direct comparison between theory and experiment since this process can be realized experimentally [7,8], while from the theoretical point of view it is a step towards realistic three-body recombination calculations for more complicated systems. Our theoretical method consists of the adiabatic hyperspherical method [9,10] and the R-matrix method [11]. The boson permutation symmetry is enforced using a modified version of the Smith-Whitten coordinate system [12,13]. Since we calculate the full S matrix, it is straightforward to also calculate the rates D_3 for the inverse process, namely, collision induced dissociation. We note that the rate equation for the density of helium atoms in a thermal gas can then be written as

$$\frac{dn_{\mathrm{He}}}{dt} = -\frac{2K_3}{6} n_{\mathrm{He}}^3 + 2D_3 n_{\mathrm{He}} n_{\mathrm{He}_2}. \tag{1}$$

We explain our method and give all necessary formulas for calculating the rates for three-body recombination and impact dissociation in Sec. II. The results are presented in Sec. III. A summary of this work is given in Sec. IV. We use atomic units throughout except where explicitly stated otherwise.

II. METHOD

We solve the Schrödinger equation for three interacting helium atoms using a combination of the adiabatic hyperspherical representation [9,10] and the R-matrix method [11]. In the adiabatic hyperspherical representation, we calculate eigenfunctions and eigenvalues of the fixed-hyperradius Hamiltonian in order to construct a set of coupled radial equations. The R-matrix method is then used in order to extract the scattering matrix from these coupled equations.

After separation of the center-of-mass motion, any three-particle system (in the absence of an external field) can be described by six coordinates. Three of these can be chosen as the Euler angles α, β, and γ that specify the orientation of the body-fixed frame relative to the space-fixed frame. The remaining three internal coordinates can be represented by a hyperradius R and two hyperangles θ and φ. To define these internal coordinates, we modify slightly the definition of the Smith-Whitten hyperspherical coordinates [12–15]. We first introduce the mass-scaled Jacobi coordinates [16]

$$\vec{\rho}_1 = (\vec{r}_2 - \vec{r}_1)/d, \tag{2}$$

$$\vec{\rho}_2 = d\left[\vec{r}_3 - \frac{m_1\vec{r}_1 + m_2\vec{r}_2}{m_1+m_2}\right] \tag{3}$$

with

 ©2002 The American Physical Society

$$d^2=\frac{(m_3/\mu)(m_1+m_2)}{m_1+m_2+m_3}, \tag{4}$$

and μ is the three-body reduced mass

$$\mu^2=\frac{m_1m_2m_3}{m_1+m_2+m_3}. \tag{5}$$

Here, $\vec{r}_i$ is the position of the particle i with mass m_i. In the case of three identical particles, we have $d=2^{1/2}/3^{1/4}$ and $\mu=m/\sqrt{3}$. We then write the hyperradius R as follows:

$$R^2=\rho_1^2+\rho_2^2, \quad R\in[0,\infty). \tag{6}$$

The hyperangles θ and φ are defined by

$$\begin{aligned}
(\vec{\rho}_1)_x&=R\cos(\theta/2-\pi/4)\sin(\varphi/2+\pi/6),\\
(\vec{\rho}_1)_y&=R\sin(\theta/2-\pi/4)\cos(\varphi/2+\pi/6),\\
(\vec{\rho}_1)_z&=0,\\
(\vec{\rho}_2)_x&=R\cos(\theta/2-\pi/4)\cos(\varphi/2+\pi/6),\\
(\vec{\rho}_2)_y&=-R\sin(\theta/2-\pi/4)\sin(\varphi/2+\pi/6),\\
(\vec{\rho}_2)_z&=0.
\end{aligned} \tag{7}$$

Here, the axes x, y, and z of the body-fixed frame are defined as follows: the z axis is parallel to $\vec{\rho}_1\times\vec{\rho}_2$, that is to say, perpendicular to the plane defined by the three particles, and the x axis is associated with the smallest moment of inertia. The hyperangles θ and φ span the ranges $[0,\pi/2]$ and $[0,2\pi]$, respectively, after requiring the wave function to be single valued [13]. The hyperangle φ can be further restricted to the range $[0,2\pi/3]$. This restriction, together with the boundary conditions given below, comes from the indistinguishability of these three particles (whether they are bosons or fermions). In addition, by our hyperangle definition in Eqs. (7), the interaction potential becomes invariant under reflections about $\varphi=\pi/3$. Therefore, in this restricted domain, the solutions of the Schrödinger equation are automatically either symmetric (bosonic) or antisymmetric (fermionic) with respect to the exchange of any two particles (see the Appendix).

We rewrite the Schrödinger equation in terms of a rescaled wave function, which is related to the usual Schrödinger solution Ψ by $\psi=R^{5/2}\Psi$. The volume element relevant to integrals over $|\psi|^2$ then becomes $2dR\sin 2\theta d\theta d\varphi d\alpha\sin\beta d\beta d\gamma$. The Schrödinger equation for three identical particles now takes the form

$$\left[-\frac{1}{2\mu}\frac{\partial^2}{\partial R^2}+\frac{\Lambda^2}{2\mu R^2}+V(R,\theta,\varphi)\right]\psi_E=E\psi_E. \tag{8}$$

In this expression, Λ^2 is the squared ''grand angular momentum operator'' and is given by [13,15]

$$\frac{\Lambda^2}{2\mu R^2}=T_\theta+T_{\varphi C}+T_r, \tag{9}$$

where

$$T_\theta=-\frac{2}{\mu R^2\sin 2\theta}\frac{\partial}{\partial\theta}\sin 2\theta\frac{\partial}{\partial\theta}, \tag{10}$$

$$T_{\varphi C}=\frac{1}{\mu R^2\sin^2\theta}\left(i\frac{\partial}{\partial\varphi}-\cos\theta\frac{J_z}{2}\right)^2, \tag{11}$$

$$T_r=\frac{J_x^2}{\mu R^2(1-\sin\theta)}+\frac{J_y^2}{\mu R^2(1+\sin\theta)}+\frac{J_z^2}{2\mu R^2}. \tag{12}$$

The operators (J_x,J_y,J_z) are the body-frame components of the total angular momentum $\vec{J}$. The interaction potential $V(R,\theta,\varphi)$ is taken to be a sum of helium dimer potentials, i.e.,

$$V(R,\theta,\varphi)=v(r_{12})+v(r_{23})+v(r_{31}), \tag{13}$$

where r_{ij} are the interparticle distances. In terms of the hyperspherical coordinates, they are

$$\begin{aligned}
r_{12}&=3^{-1/4}R[1+\sin\theta\sin(\varphi-\pi/6)]^{1/2},\\
r_{23}&=3^{-1/4}R[1+\sin\theta\sin(\varphi-5\pi/6)]^{1/2},\\
r_{31}&=3^{-1/4}R[1+\sin\theta\sin(\varphi+\pi/2)]^{1/2}.
\end{aligned} \tag{14}$$

For the helium dimer potential we use the representation of Aziz *et al.*, designated HFD-B3-FCI1 [6].

The first step that must be carried out is the solution of the fixed-R adiabatic eigenvalue equation for a given symmetry J^Π to determine the adiabatic eigenfunctions (or channel functions) and eigenvalues (or potential curves). The adiabatic eigenfunction representation writes the wave function $\psi_E(R,\Omega)$ [we will write $\Omega\equiv(\theta,\varphi,\alpha,\beta,\gamma)$] in terms of the complete, orthonormal set of angular wave functions Φ_ν and radial wave functions $F_{\nu E}$,

$$\psi_E(R,\Omega)=\sum_\nu F_{\nu E}(R)\Phi_\nu(R;\Omega). \tag{15}$$

The channel functions Φ_ν are eigenfunctions of the five-dimensional partial differential equation

$$\left[\frac{\Lambda^2}{2\mu R^2}+\frac{15}{8\mu R^2}+V(R,\theta,\varphi)\right]\Phi_\nu(R;\Omega)=U_\nu(R)\Phi_\nu(R;\Omega), \tag{16}$$

whose solutions depend parametrically on R. Insertion of ψ_E from Eq. (15) into the Schrödinger equation from Eq. (8) results in a set of coupled ordinary differential equations

$$\left[-\frac{1}{2\mu}\frac{d^2}{dR^2}+U_\nu(R)\right]F_{\nu E}(R)-\frac{1}{2\mu}\sum_{\nu'}\left[2P_{\nu\nu'}(R)\frac{d}{dR}+Q_{\nu\nu'}(R)\right]F_{\nu' E}(R)=EF_{\nu E}(R). \tag{17}$$

The coupling elements $P_{\nu\nu'}(R)$ and $Q_{\nu\nu'}(R)$ involve partial first and second derivatives of the channel functions Φ_ν with respect to R, and are defined as follows:

$$P_{\nu\nu'}(R)=\left\langle\left\langle \Phi_\nu(R;\Omega)\left|\frac{\partial}{\partial R}\right|\Phi_{\nu'}(R;\Omega)\right\rangle\right\rangle \tag{18}$$

and

$$Q_{\nu\nu'}(R)=\left\langle\left\langle \Phi_\nu(R;\Omega)\left|\frac{\partial^2}{\partial R^2}\right|\Phi_{\nu'}(R;\Omega)\right\rangle\right\rangle. \tag{19}$$

The double-bracket matrix element signifies that integrations are carried out only over the angular coordinates Ω. These nonadiabatic couplings can peak sharply at avoided crossings, leading to numerical difficulties when solving the coupled equations (17) based on the adiabatic basis expansion. As we will see in Sec. III, however, the sharp avoided crossings among the channels we consider occur at small R at energies several orders of magnitude larger than the collision energies considered (more than 10^{-4} a.u. compared to a few millikelvin $\sim 10^{-9}$ a.u.). This crossing is thus well into the classically forbidden region where the wave functions are vanishingly small. These considerations combined with our use of a global numerical method rather than a propagation method lead to the conclusion that this crossing has no significant effect on our calculations.

In order to solve the adiabatic equation (16), we expand the channel function on Wigner D functions

$$\Phi_\nu^{JM\Pi}(R;\Omega)=\sum_K \phi_{K\nu}(R;\theta,\varphi)D^J_{KM}(\alpha,\beta,\gamma). \tag{20}$$

The quantum numbers K and M denote the projections of $\vec{J}$ onto the body-fixed and space-fixed z axes, respectively. K takes the values $J, J-2, \ldots, -(J-2), -J$ for the "parity-favored" case, $\Pi=(-1)^J$, and $J-1, J-3, \ldots, -(J-3), -(J-1)$ for the "parity-unfavored" case, $\Pi=(-1)^{J+1}$, since K should be even for even parity and odd for odd parity [13]. The resulting complex coupled equations in θ and φ are solved by expanding $\phi_{K\nu}(R;\theta,\varphi)$ onto a direct product of fifth-order basis splines [18] in θ and φ. We generate the basis splines for θ from 50 mesh points, while we use 80 mesh points for φ. This leads, for example, to a basis size of 17 712 in the case of the 3^- symmetry. Typically, a calculation of the 30 lowest eigenvalues of the adiabatic equation (16) takes about 20 min of CPU time on a 500-MHz alpha EV6 workstation.

The identical particle symmetry was built into the adiabatic equations via the boundary conditions (see the Appendix)

$$\Phi_\nu(R;\theta,\varphi=0,\alpha,\beta,\gamma) = \pm\Phi_\nu\left(R;\theta,\varphi=\frac{2\pi}{3},\alpha,\beta,\gamma\right) \quad \text{for } \Pi=\pm 1. \tag{21}$$

These conditions ensure that each solution is either symmetric or antisymmetric with respect to the exchange of any two particles (about half of the solutions are symmetric), thus eliminating all states of mixed symmetry. The symmetric channel functions appropriate for identical bosons are then extracted in a postsymmetrization procedure as the solutions that satisfy

$$\left\langle\left\langle \Phi_\nu(R;\Omega)\left|\frac{1+P_{23}}{2}\right|\Phi_\nu(R;\Omega)\right\rangle\right\rangle=1. \tag{22}$$

In practice we solve the adiabatic equation (16) for a set of about 140 radial grid points R_i up to $R\approx 1400$ a.u. in order to obtain the potential curves $U_\nu(R)$ and the coupling matrix elements $P_{\nu\nu'}(R)$ and $Q_{\nu\nu'}(R)$; for $R>1400$ a.u. they are calculated by an extrapolation procedure. The $P_{\nu\nu'}(R)$ and $Q_{\nu\nu'}(R)$ are calculated with a simple differencing scheme, i.e.,

$$\frac{\partial}{\partial R}\Phi_\nu(R;\Omega)\approx\frac{\Phi_\nu(R+\Delta R;\Omega)-\Phi_\nu(R-\Delta R;\Omega)}{2\Delta R}. \tag{23}$$

We tested this seemingly crude formula by calculating $P_{\nu\nu'}(R)$ and $Q_{\nu\nu'}(R)$ for several values of ΔR and found that they are stable to at least four significant digits. The accuracy of $P_{\nu\nu'}(R)$ has also been verified by comparing them with those calculated using the Hellmann-Feynman formula $P_{\nu\nu'}(R)=\langle\langle\Phi_\nu|\partial H_{\rm ad}/\partial R|\Phi_{\nu'}\rangle\rangle/[U_{\nu'}(R)-U_\nu(R)]$.

The Φ_ν are *a priori* complex quantities that may have arbitrary phases upon numerical diagonalization. While their overall phase is not important, a consistent phase convention is required in order for $P_{\nu\nu'}(R)$ and $Q_{\nu\nu'}(R)$ to be continuous in R. Therefore, we require that the projection of the channel functions onto the lowest hyperspherical harmonic be real. If their projection equals zero, their phase is fixed using the second lowest hyperspherical harmonic instead. These hyperspherical harmonics, which are the eigenfunctions of the squared grand angular momentum operator Λ^2, should be calculated using the same boundary conditions given in Eq. (21). The channel functions have now been determined only up to an overall sign. Thus, the additional condition $\mathrm{Re}\langle\langle\Phi_\nu(R_i;\Omega)|\Phi_\nu(R_{i+1};\Omega)\rangle\rangle>0$ is imposed. Our experience indicates that the coupling matrix elements $P_{\nu\nu'}(R)$ and $Q_{\nu\nu'}(R)$ become purely real quantities with this phase convention.

We solve the coupled equations (17) using the adiabatic finite element method (FEM) [19]. About 10^4 FEM sectors, in each of which fifth-order polynomials are used to expand the radial wave function, extend from $R=5$ to 5×10^5 a.u., and 12 adiabatic channels are used. The scattering S matrix is

then extracted using the *R*-matrix method [11]. Each energy took about 4 min of CPU time on a 500-MHz alpha EV6 workstation.

We adopt the convention of Mott and Massey [20] in defining the cross section σ_3 for three identical particle collisions as the ratio of the scattered radial flux to the incident flux in only *one* of the six symmetrizing permutations of the incident plane wave [1]. The total event rate constant for three-body recombination is then expressed as (the conversion from a.u. to cm^6/s is 1 a.u. $=9.078\,05\times10^{-34}$ cm^6/s)

$$K_3=\frac{k}{\mu}\sigma_3^K=\sum_{J,\Pi} K_3^{J\Pi}, \tag{24}$$

where $K_3^{J\Pi}$ is the partial recombination rate corresponding to the J^Π symmetry

$$K_3^{J\Pi}=\sum_{i,f}\frac{192(2J+1)\pi^2}{\mu k^4}|S_{f\leftarrow i}^{J\Pi}|^2. \tag{25}$$

Here, i and f label the incident (three-body continuum) and outgoing (two-body recombination) channels, respectively, and $k=(2\mu E)^{1/2}$ are the hyperradial wave numbers in the incident channels. The case of helium atoms is simple, since there is only one two-body recombination channel in the sum of Eq. (25). This generalized cross section σ_3^K has units of $(\mathrm{length})^5$, as is appropriate to characterize scattering in six dimensions.

On the other hand, the collision induced dissociation rate is expressed as (the conversion from a.u. to cm^3/s is 1 a.u. $=6.126\,15\times10^{-9}$ cm^3/s)

$$D_3=\frac{k_{12,3}}{\mu_{12,3}}\sigma_3^D=\sum_{J,\Pi} D_3^{J\Pi}, \tag{26}$$

where the partial dissociation rate is given by

$$D_3^{J\Pi}=\sum_{i,f}\frac{(2J+1)\pi}{\mu_{12,3}k_{12,3}^i}|S_{f\leftarrow i}^{J\Pi}|^2. \tag{27}$$

Here, i and f correspond to the two-body and three-body channels, respectively, $\mu_{12,3}=2m/3$ is the two-body reduced mass, $k_{12,3}^i=[2\mu_{12,3}(E-E_{12}^i)]^{1/2}$ is the two-body wave number, and E_{12}^i is the two-body binding energy. This expression differs from Eq. (25) in two ways. The first is that since the initial state is a two-body channel instead of a three-body channel, the cross section needs to be divided by $(k_{12,3}^i)^2$ rather than k^5 ($k_{12,3}^i$ and k^4 in the rate). The second is that the factor 192 is absent. This factor comes from the product of the symmetrization factor for the three identical particles, $3!=6$, and the factor $32\pi^2$ for the usual three-body collision cross-section formula.

III. RESULTS AND DISCUSSION

Since the ^{4}He dimer has only a single $l=0$ bound state, three-body recombination is allowed only for the parity-favored cases, that is, $\Pi=(-1)^J$. Figure 1 shows the two lowest potential curves for the $J^\Pi=0^+,1^-,2^+$, and 3^- symmetries. For each case the lowest curve asymptotically corresponds to two atoms bound in a dimer, with the third atom far away. The asymptotic value of these potentials equals the two-body binding energy $E_{12}=-5.0\times10^{-9}$ a.u. The second channel for each symmetry corresponds to the lowest three-body continuum state, i.e., all three atoms far away from each other. Recall that in the adiabatic hyperspherical representation the three-body continuum is rigorously discretized since the adiabatic Hamiltonian depends only on the bounded hyperangles. These three-body continuum channel functions converge asymptotically to the hyperspherical harmonics. Therefore, the corresponding potential curves behave as

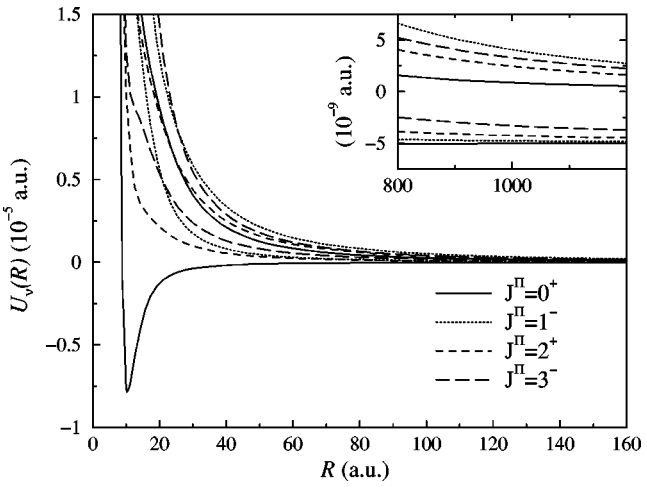

FIG. 1. Two lowest potential curves for the $J^\Pi=0^+,1^-,2^+$, and 3^- symmetries. The inset shows the asymptotic behavior of these potential curves.

$$U_\nu(R)\to\frac{\lambda(\lambda+4)+\frac{15}{4}}{2\mu R^2}\quad\text{for } R\to\infty. \tag{28}$$

In principle, λ can take on any non-negative integer value, but the requirements of permutation symmetry limit its minimum value, $\lambda_{\min}=0$, 3, 2, and 3 for $J^\Pi=0^+$, 1^-, 2^+, and 3^-, respectively. Knowing the asymptotic form of the hyperradial potentials allows a generalization of Wigner's threshold law [17], leading to the partial recombination rates

$$K_3^{J\Pi}\propto E^{\lambda_{\min}} \tag{29}$$

and the partial dissociation rates

$$D_3^{J\Pi}\propto E^{\lambda_{\min}+2} \tag{30}$$

near threshold. The different threshold energy dependencies can be traced to energy denominators in Eqs. (25) and (27) since both use the same *S*-matrix element.

Recombination and dissociation occur via nonadiabatic couplings between the two-body recombination channel and three-body continuum channels. A useful parametrization of this coupling is the unitless ''nonadiabatic coupling strength,'' defined as the ratio of the squared coupling matrix

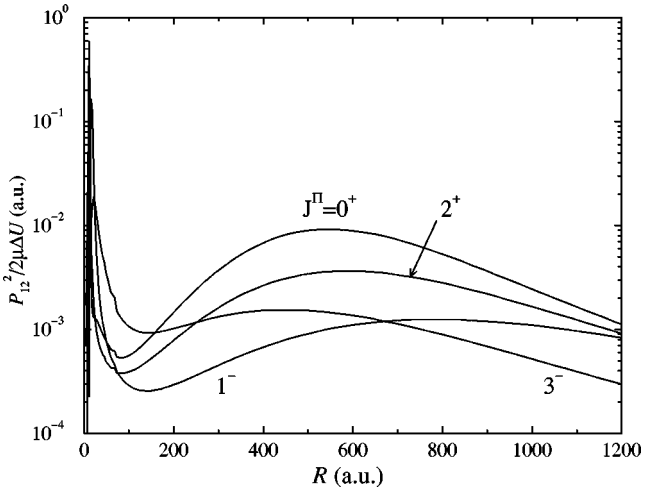

FIG. 2. Nonadiabatic coupling strengths between the lowest and the second lowest channels for the $J^\Pi=0^+$, 1^-, 2^+, and 3^- symmetries.

element $P_{\nu\nu'}(R)^2$ to the product of the difference in the adiabatic curves $\Delta U(R)=U_{\nu'}(R)-U_\nu(R)$ and the reduced mass μ. Figure 2 shows the nonadiabatic coupling strengths between the lowest two channels for the $J^\Pi=0^+,1^-,2^+$, and 3^- symmetries. The nonadiabatic couplings are important for $R=10$–40 a.u. and for $R=300\sim800$ a.u., but recombination and dissociation occur mainly in the latter range. The peak $J^\Pi=0^+$ is located around $R\sim3a$, with the helium two-body scattering length $a=172$ a.u., as is expected from Refs. [1,3]. It is interesting to note that the peak position for higher J's does not appear to follow any systematic trend with either J or $\lambda_{\min}$.

Figure 3 shows the total three-body recombination rate K_3 as well as the partial recombination rates $K_3^{J\Pi}$ for the $J^\Pi=0^+$, 1^-, 2^+, and 3^- symmetries as a function of the collision energy. At the lower collision energies, the partial recombination rates behave as $E^{\lambda_{\min}}$, as predicted by Wigner's

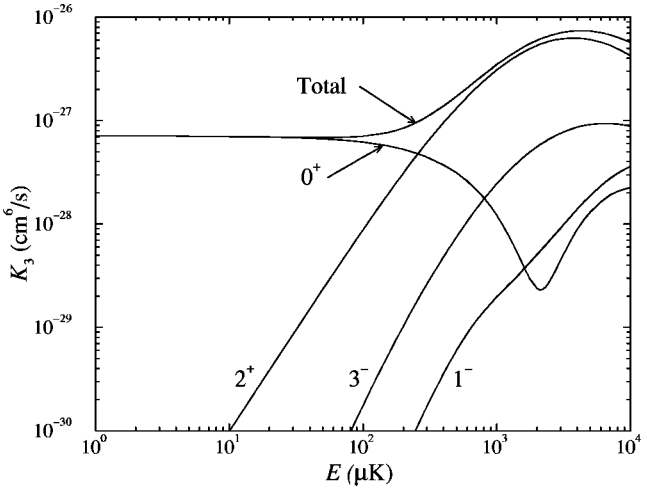

FIG. 3. Total three-body recombination rate K_3 as well as partial recombination rates $K_3^{J\Pi}$ for the $J^\Pi=0^+,1^-,2^+$, and 3^- symmetries as a function of the collision energy.

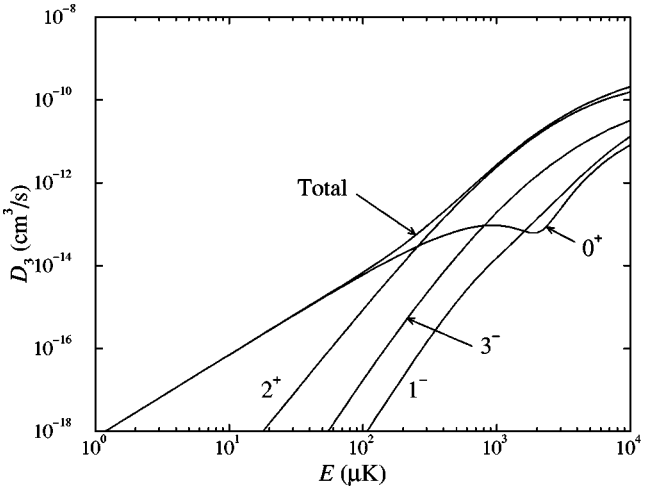

FIG. 4. Total collision induced dissociation rate D_3 as well as partial dissociation rates $D_3^{J\Pi}$ for the $J^\Pi=0^+$, 1^-, 2^+, and 3^- symmetries as a function of the collision energy (with respect to the three-body continuum threshold).

law, Eq. (29) [17]. In the ultracold limit, here $E<30$ μK, the total recombination rate K_3 is constant, and the 0^+ partial recombination rate dominates. For this symmetry, the Stückelberg minimum is not as deep as that found in Ref. [3]. This difference can be understood from the fact that they included only one three-body continuum channel, which permits completely destructive interference within their two channel calculation. The present calculation, on the other hand, includes 11 continuum channels, resulting in less than completely destructive interference.

Figure 4 shows the total collision induced dissociation rate D_3 as well as the partial dissociation rates $D_3^{J\Pi}$ for the $J^\Pi=0^+$, 1^-, 2^+, and 3^- symmetries as a function of the collision energy (with respect to the three-body continuum threshold). At the lower collision energies, the partial recombination rates behave as $E^{\lambda_{\min}+2}$, as predicted by Wigner's law. As for recombination, the partial dissociation rate corresponding to the 0^+ symmetry dominates for $E<30$ μK.

Finally, to facilitate future comparison with experimental data, Table I gives the values for the total recombination and dissociation rates as functions of the energy. We have checked the stability of the results with respect to the final matching distance, the number of FEM sectors, and the number of coupled channels, and have found our results accurate to the two significant figures given.

IV. SUMMARY

In this work, we have generalized our earlier work to calculate the rates for three-body recombination and collision induced dissociation at nonzero collision energies. Although we have calculated the recombination and dissociation rates for $E<10$ mK, those for higher energies can be obtained by including higher J states. We expect that at 10 mK our results are sufficiently accurate, because for the next contributing symmetry $J^\Pi=4^+$, $\lambda_{\min}$ is equal to 4, leading to recombination and dissociation rates much smaller than those

TABLE I. Recombination rate and collision induced dissociation rate as a function of the collision energy.

E (μK)	K_3 (cm^6/s)	D_3 (cm^3/s)
1	7.1×10^{-28}	7.1×10^{-19}
3	7.1×10^{-28}	6.4×10^{-18}
5	7.1×10^{-28}	1.8×10^{-17}
7	7.0×10^{-28}	3.4×10^{-17}
10	7.0×10^{-28}	7.0×10^{-17}
30	6.9×10^{-28}	6.2×10^{-16}
50	6.9×10^{-28}	1.7×10^{-15}
70	6.9×10^{-28}	3.3×10^{-15}
100	7.1×10^{-28}	6.8×10^{-15}
300	1.1×10^{-27}	8.9×10^{-14}
500	1.1×10^{-27}	3.7×10^{-13}
700	2.4×10^{-27}	9.9×10^{-13}
1000	3.5×10^{-27}	2.7×10^{-12}
3000	7.0×10^{-27}	3.7×10^{-11}
5000	7.3×10^{-27}	8.8×10^{-11}
7000	6.7×10^{-27}	1.4×10^{-10}
10000	5.7×10^{-27}	2.1×10^{-10}

for lower J's. We have considered the relatively simple case of ground-state helium atoms, as it is one of the few physical systems for which rigorous calculations can currently be carried out. Its simplicity is a result of the single two-body recombination channel. While we have neglected the three-body term in the interaction potential, its inclusion would not complicate our approach. For heliums atoms, however, the three-body term is expected to play only a minor role. We thus hope that our results will allow a direct comparison with future experimental data. With further improvements, extensions may be possible to the more complicated cases of spin-polarized alkali atoms such as H and Li, where the large number of two-body recombination channels currently poses difficulties.

ACKNOWLEDGMENTS

This research was supported in part by the National Science Foundation, and the computing was supported by the Research Corporation. J.P.B. acknowledges support from the National Research Council.

APPENDIX: BOUNDARY CONDITIONS

The boundary conditions, Eq. (21), can be derived by imposing the continuity condition required for Smith-Whitten hypersherical coordinates [13],

$$\Phi_\nu(R;\theta,\varphi,\alpha,\beta,\gamma)=\Phi_\nu(R;\theta,\varphi+2\pi,\alpha,\beta,\gamma+\pi), \tag{A1}$$

and by applying the symmetrization operator

$$\mathcal{S}=1+P_{12}+P_{23}+P_{31}+P_{12}P_{31}+P_{12}P_{23} \tag{A2}$$

TABLE II. Effects of permutation operations on the hyperangle φ and the Wigner D function.

Permutation	φ	D^J_{KM}
P_{12}	$\frac{4\pi}{3}-\varphi$	$(-1)^{J+K}D^J_{-KM}$
P_{23}	$\frac{2\pi}{3}-\varphi$	$(-1)^{J}D^J_{-KM}$
P_{31}	$2\pi-\varphi$	$(-1)^{J}D^J_{-KM}$
$P_{12}P_{31}$	$\varphi+\frac{2\pi}{3}$	$(-1)^{K}D^J_{KM}$
$P_{12}P_{23}$	$\varphi+\frac{4\pi}{3}$	D^J_{KM}

to the channel functions. For this purpose, it is convenient to consider basis functions of the form

$$\Phi^{J\Pi M}_{lm}(\Omega)=f_l(\theta)e^{im\varphi}D^J_{KM}(\alpha,\beta,\gamma) \tag{A3}$$

rather than the basis splines in θ and φ that were actually used in the computation. The effects of the permutation operations in Eq. (A2) are shown in Table II [it is not difficult to see that the interaction potential (13) is invariant under these operations]. The continuity condition in Eq. (A1) leads to the condition that $K/2+m$ must be integral. Thus, for even parity $\Pi=+1$, or K even, m must be integral, while for odd parity $\Pi=-1$, or K odd, m must be half integral. The application of $\mathcal{S}$ to the functions (A3) leads to

$$\begin{aligned}\mathcal{S}\Phi^{J\Pi M}_{lm}(\Omega)=f_l(\theta)&[1+e^{i(2\pi/3)m}(-1)^K+e^{i(4\pi/3)m}]\\&\times[e^{im\varphi}D^J_{KM}+(-1)^J(-1)^{i(2\pi/3)m}\\&\times e^{-im\varphi}D^J_{-KM}].\end{aligned} \tag{A4}$$

These quantities vanish unless

$$\begin{aligned}m&=3n \quad \text{for } \Pi=+1,\\ m&=3n+\frac{3}{2} \quad \text{for } \Pi=-1,\end{aligned} \tag{A5}$$

where n is any integer. In other words, the φ dependence of the basis functions should take the form $e^{i3n\varphi}$ for $\Pi=+1$ and $e^{i(3n+3/2)\varphi}$ for $\Pi=-1$. These functions obey the boundary conditions given in Eq. (21) for each parity, allowing the application of the boundary conditions themselves. Unfortunately, the application of the antisymmetrization operator $\mathcal{A}=1-P_{12}-P_{23}-P_{31}+P_{12}P_{31}+P_{12}P_{23}$ to the functions (A3) leads to the same boundary conditions. Thus, after solving the adiabatic equation (16), we must extract the bosonic solutions. In practice, this postsymmetrization is accomplished by checking the effect of P_{23} on the solutions of the adiabatic equation (16).

[1] B.D. Esry, C.H. Greene, and J.P. Burke, Jr., Phys. Rev. Lett. **83**, 1751 (1999).
[2] P.O. Fedichev, M.W. Reynolds, and G.V. Shlyapnikov, Phys. Rev. Lett. **77**, 2921 (1996).
[3] E. Nielsen and J.H. Macek, Phys. Rev. Lett. **83**, 1566 (1999).
[4] P.F. Bedaque, E. Braaten, and H.-W. Hammer, Phys. Rev. Lett. **85**, 908 (2000).
[5] E. Braaten and H.-W. Hammer, Phys. Rev. Lett. **87**, 160407 (2001).
[6] R.A. Aziz, A.R. Janzen, and M.R. Moldover, Phys. Rev. Lett. **74**, 1586 (1995).
[7] W. Schöllkopf and J.P. Toennies, Science **266**, 1345 (1994).
[8] W. Schöllkopf and J.P. Toennies, J. Chem. Phys. **104**, 1155 (1996).
[9] B.D. Esry, C.D. Lin, and C.H. Greene, Phys. Rev. A **54**, 394 (1996).
[10] C.D. Lin, Phys. Rep. **257**, 1 (1995).
[11] M. Aymar, C.H. Greene, and E. Luc-Koenig, Rev. Mod. Phys. **68**, 1015 (1996).
[12] B.R. Johnson, J. Chem. Phys. **73**, 5051 (1980).
[13] B.K. Kendrick, R.T. Pack, R.B. Walker, and E.F. Hayes, J. Chem. Phys. **110**, 6673 (1999).
[14] R.C. Whitten and F.T. Smith, J. Math. Phys. **9**, 1103 (1968).
[15] B. Lepetit, Z. Peng, and A. Kuppermann, Chem. Phys. Lett. **166**, 572 (1990).
[16] L.M. Delves, Nucl. Phys. **9**, 391 (1958); **20**, 275 (1960).
[17] B.D. Esry, C.H. Greene, and H. Suno, Phys. Rev. A (to be published).
[18] C. de Boor, *A Practical Guide to Splines* (Springer, New York, 1978).
[19] J.P. Burke, Jr., Ph.D. thesis, University of Colorado, 1999.
[20] N.F. Mott and H.S.W. Massey, *The Theory of Atomic Collisions* 3rd ed. (Clarendon Press, Oxford, 1965), pp. 294–300.